Rayleigh scattering by atomic ions of low nuclear charge

G. Basavaraju,* Lynn Kissel,† John C. Parker, R. H. Pratt, S. C. Roy,‡ and S. K. Sen Gupta§
Department of Physics and Astronomy, University of Pittsburgh, Pittsburgh, Pennsylvania 15260
(Received 25 April 1986)

Rayleigh scattering amplitudes and elastic photon-atom scattering cross sections have been calculated for C^0, C^{1+}, C^{2+}, C^{4+}, Ne^0, Ne^{1+}, Ne^{2+}, Ne^{4+}, Ne^{6+}, Ne^{8+}, and Ne^{9+} atoms and ions in their ground state. Some data were also obtained for oxygen. X-ray energies considered are in the regions above and below the threshold energy for K-shell photoionization. Except in the immediate neighborhood of this threshold energy, the primary effect of ionization on the atomic cross section is to reduce the number of electrons from which scattering occurs. The resonance region near threshold widens with increasing ionization, as with vacancies in deeper-lying states transitions to intermediate states further below threshold are allowed. Above the threshold energy, K-shell amplitudes in an isonuclear sequence, except for hydrogenlike-ion cases, share a common curve differing only in the position of the threshold. Further, when the photon energy is expressed in units of the K-shell threshold energy, both carbon and neon imaginary amplitudes share a common curve. Well above the threshold, the real part of amplitudes approach form-factor predictions.

I. INTRODUCTION

The variation of photon-interaction cross sections for excited and ionized states of atoms is of interest for plasma physics. We report in this paper calculations of photon elastic scattering by low Z atoms (C, O, and Ne) in different ionization states (C^0, C^{1+}, C^{2+}, C^{4+}, C^{5+}, O^0, O^{1+}, O^{6+}, O^{7+}, Ne^0, Ne^{1+}, Ne^{2+}, Ne^{4+}, Ne^{6+}, Ne^{8+}, and Ne^{9+}). We consider photon energies in the x-ray range, i.e., both above and below the K-shell ionization threshold (ω_K) of these light atoms. At these energies elastic scattering is essentially Rayleigh scattering—the scattering by bound atomic electrons. Ionization reduces the number of bound electrons from which scattering can occur and correspondingly reduces the total scattering cross section. However, as can be seen from Figs. 1 and 2, ionization also brings about rather different detailed variations in the cross section in the near vicinity of the K edge.

The atomic elastic scattering amplitude is a coherent sum of the scattering amplitudes from the bound electrons. We therefore begin by examining effects of ionization on scattering from individual bound electrons (to be more precise, subshells) and then consider consequences for the coherent sum.

If the wave vectors of the photons in the initial and final states are denoted, respectively, by $\mathbf{k}_i$ and $\mathbf{k}_f$, and the corresponding polarization vectors by $\mathbf{e}_i$ and $\mathbf{e}_f$, then the general form of the Rayleigh scattering matrix element for coherent scattering from a closed subshell is

$$M = A(\mathbf{e}_i \cdot \mathbf{e}_f^*) + B(\mathbf{e}_i \cdot \boldsymbol{\nu}_f)(\mathbf{e}_f^* \cdot \boldsymbol{\nu}_i) \ . \tag{1}$$

Here the amplitudes A and B are complex quantities which depend on the photon energy (ω) and the scattering angle θ, and $\boldsymbol{\nu}_i$ and $\boldsymbol{\nu}_f$ are unit vectors along $\mathbf{k}_i$ and $\mathbf{k}_f$, respectively. If $\mathbf{e}_i$ is perpendicular (parallel) to the scattering plane defined by $\mathbf{k}_i$ and $\mathbf{k}_f$, $\mathbf{e}_f$ must also be perpendicular (parallel) to the scattering plane. We may define the alternative set of amplitudes

$$A_{\perp} \sim A \text{ and } A_{\parallel} \sim A\cos\theta - B\sin^2\theta \ ,$$

corresponding to these situations. The atomic differential scattering cross section, summed over the final photon polarizations and averaged over the initial ones, is

$$\frac{d\sigma}{d\Omega} = \frac{r_0^2}{2}(|A_{\perp}|^2 + |A_{\parallel}|^2) \ , \tag{2}$$

where $r_0 = e^2/mc^2$ is the classical electron radius. In the

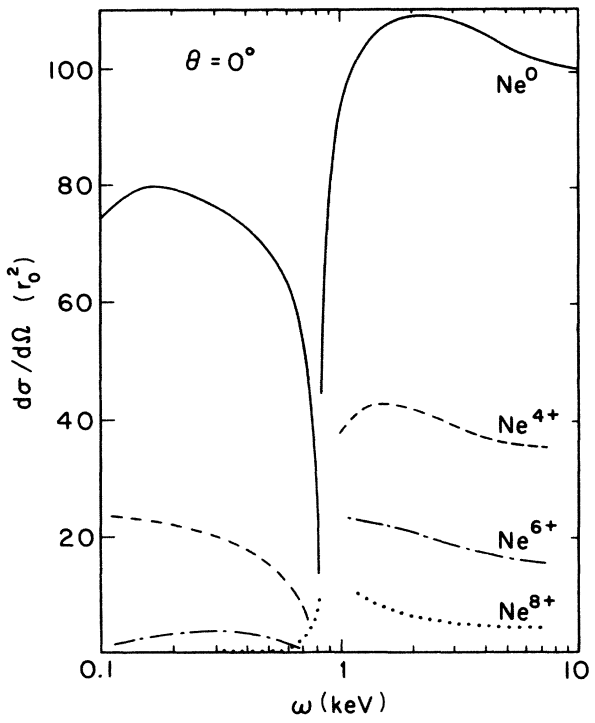

FIG. 1. Comparison of total atom elastic scattering cross sections for different degrees of ionization, in Ne. The details in the resonance region are deleted.

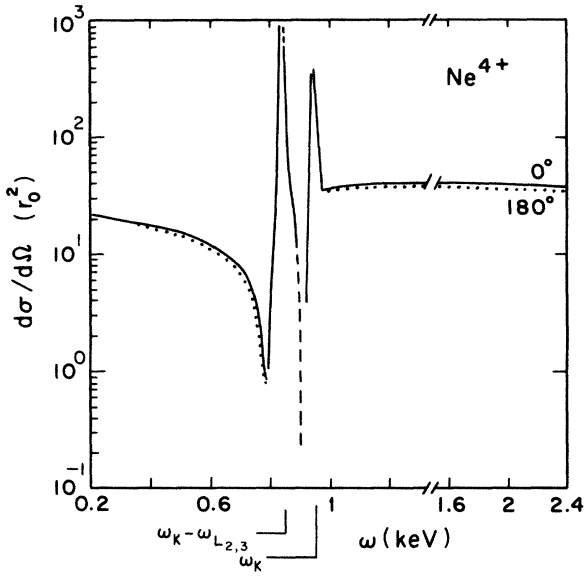

FIG. 2. Total atom elastic scattering cross sections for Ne^{4+} showing some details in the resonance region. (——) forward scattering; (— — —) 180° backward scattering.

present energy regime, we find that $A_{\parallel}$ is generally equal to $A_{\perp}\cos\theta$, implying the smallness of B. The variation of $A_{\perp}$ with θ is small until $\omega \geq 2\omega_K$. Our major discussion in this paper will therefore be in terms of the forward amplitude $A_{\perp}$ and the forward scattering cross section.

In our work the Rayleigh scattering amplitudes are obtained numerically in the independent-particle approximation through the calculation, in partial waves and multipoles, of the second-order S-matrix element in a relativistic screened self-consistent central potential. The details of the numerical procedures have been given previously.[1-3] For neutral atoms it appears that, except perhaps very close to thresholds, there are no major discrepancies between theory and experiment, at least in the x-ray and low-energy γ-ray regime.[4]

For photon energies well above ω_K the K-shell amplitude is a monotonically decreasing function of ω. In an isonuclear sequence, except for the extreme case of the hydrogenlike ion, the amplitudes share a common curve. Further, when photon energy is expressed in units of ω_K, carbon, oxygen, and neon imaginary amplitudes share a common curve, implying the applicability of a common scaled potential at large distances from the nucleus. For photon energies less than ω_K the amplitudes exhibit resonances at ω corresponding to bound-bound transitions. For the K shell amplitude, these resonances are just below ω_K and the resonance region expands with increasing ionization due to increasing separation between the bound-state energies. As $\omega \to 0$ the amplitudes approach zero as ω^2 for small ω. These aspects of K shell amplitudes are discussed in Sec. II.

For L-shell amplitudes, resonances occur in two different regions. One region, analogous to that in the K shell, is just below the L-shell photoionization threshold. In light elements, this energy region occurs below 100 eV, with a width no more than a few eV. The features of such resonances are expected to be similar to those in the K amplitudes and are not examined in the present study. However, a second energy region in which the L shell amplitudes show resonances is near ω_K, corresponding to the energy of bound-bound transition from the L shell to the K shell. These sometimes "spurious" resonances are the counterparts of the corresponding $K \to L$ transition resonances in the K-shell amplitude. When both subshells are full, these two resonance contributions cancel exactly. L-shell amplitudes are discussed in Sec. III.

In Sec. IV, the total atom amplitudes and the corresponding cross sections are considered. The relevance of the resonances in the shellwise amplitudes is discussed. For atoms in which L_2 and L_3 subshells are filled or partially filled, some of the resonances in the K shell amplitude are canceled or partially canceled by the counterpart resonances in L_2 and L_3 amplitudes. Nevertheless, in these light elements (for which the M shell is not full) the resonances in the K-shell amplitude corresponding to $K \to M$ transitions manifest themselves when they interfere with slowly varying amplitudes by causing the cross section to go through a well-defined minimum before the resonance region below ω_K. The depth of this minimum depends on the atom. If the L_2 and L_3 subshells are not full, the corresponding resonances in the K-shell amplitude manifest themselves as multiple maxima and minima in the atomic cross sections. In Sec. V, some features of the angular dependence of the amplitudes and the cross sections are mentioned.

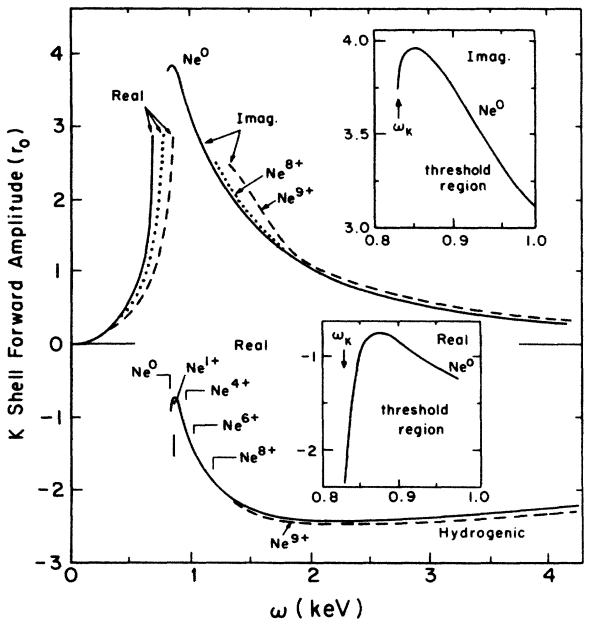

FIG. 3. Real and imaginary parts of the Rayleigh forward scattering amplitude from the K shell for different neon ions. The resonance region between 0.7 and ~1.0 keV has been deleted for the sake of clarity; the region just above threshold for Ne^0 has been enlarged in the panels. Note how the Ne^{9+} case distinctly stands out from the rest.

II. K-SHELL AMPLITUDE

First we consider the general features of K-shell amplitudes as displayed in Figs. 3 and 4. In these figures, which show forward amplitudes, the behavior in the region immediately below ω_K has been deleted. This deleted region has special and complex features, which will be considered subsequently. At very low energies, below about 200 eV, the amplitudes have the expected variation, namely they approach zero as ω^2 for small ω. As ω increases the amplitude at a given ω is less as ionization increases. This is largely due to the increased value of $\omega_K - \omega_L$ for increasing ionization, shifting the resonance to higher energy. The steeply rising portion is actually the "wing" region of the $K \rightarrow L_{2,3}$ resonance.

In the energy regime $\omega > \omega_K$, the amplitude is complex. We see that the real and imaginary parts for an isonuclear sequence with filled K shells (C^0 to C^{4+}, O^0 to O^{6+}, and Ne^0 to Ne^{8+}) share a common curve. Only the position of the threshold varies, moving to higher energy with increasing ionization. However, when the K shell has been opened, as in Ne^{9+}, O^{7+}, and C^{5+}, the amplitude, giving due consideration to the halved occupation (i.e., amplitude per electron) increases in magnitude. This is to be understood because the potential in the vicinity of the K shell is practically unaltered by the ionization of L-shell electrons; only the removal of a K-shell electron (so that the remaining electron is in a pure point Coulomb potential) brings about a noticeable (though not large) change.

In Fig. 5, K-shell amplitudes for neon, oxygen, and carbon are plotted against photon energy in units of neutral K-shell threshold energy. We see that in the case of the imaginary part, except very close to $\omega/\omega_K = 1$, the data for the three elements differ very little. In fact only for Ne^{9+} (not shown) are there differences (1–3%) from the rest of the neon data. However, in the case of the real part, the difference between the elements is significant over a larger range of energy. Since the imaginary parts of the amplitudes are related to cross sections for real transitions to the intermediate continuum states, the sharing of a common curve implies applicability of a scaled potential at the distances which characterize such transitions. The real anomalous amplitudes, however, are determined in part (through the dispersion relations) in terms of bound-bound transitions sensitive to distances which do not scale.

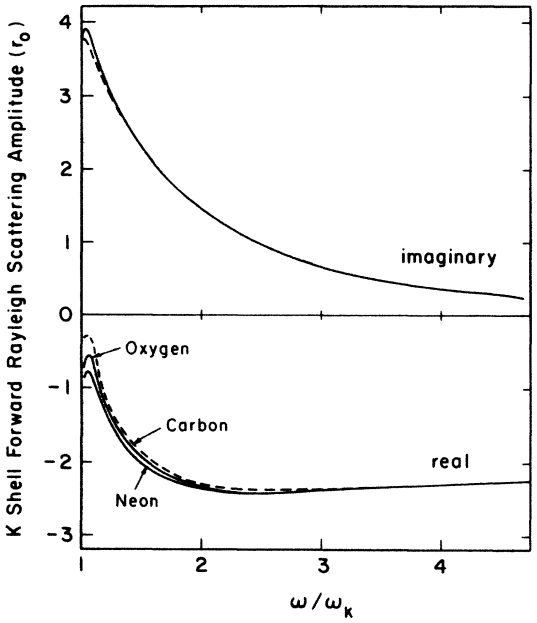

FIG. 5. Real and imaginary parts of K-shell forward amplitudes plotted as a function of ω/ω_K. Hydrogenic ions have not been included.

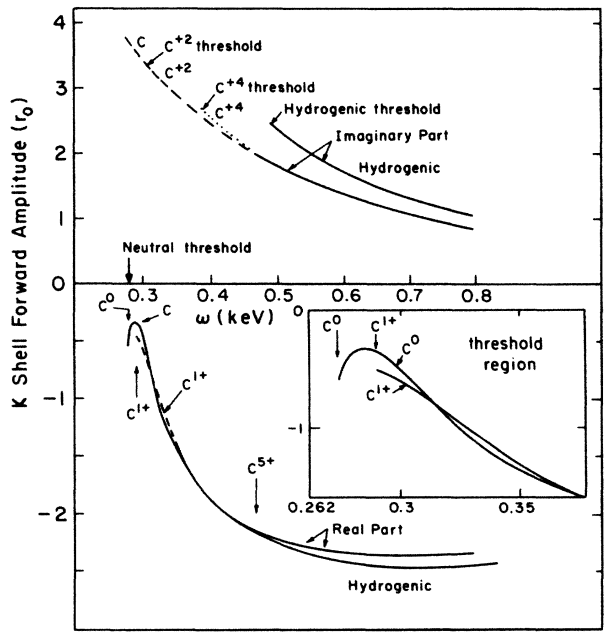

FIG. 4. Same as in Fig. 3, but for carbon ions.

The statements in the foregoing paragraphs are only valid for photon energies not too close to threshold (not within about 50–80 eV). Close to threshold there are significant differences in the amplitudes for different ions of the same element, reflecting differences in the exterior regions of the potentials. The "turnaround" behavior of the C real part is absent in the case of the carbon ions. The kink in the imaginary part of C^0 is noticeable in C^{1+} but not present in the other carbon ions. (The same kink is seen in direct calculations utilizing codes written to calculate photoelectric effect.) The "turnaround" of the real amplitudes is more pronounced for O^0 and O^{1+}, still more pronounced in neon, but is still not seen in the more highly ionized species. It may be remarked that the hydrogenic nonrelativistic dipole approximation (NRDA) calculation of Gavrila[5] predicts only smooth behaviors of the amplitudes, as was generally found in the case of most ions. The special threshold features of neutral atom and weakly ionized cases require further investigation.

In the second-order S-matrix formalism for the Rayleigh scattering process there is a summation over intermediate states: other bound states and continuum states. Since each subshell amplitude is calculated independently of the occupation of other subshells, all single-photon

bound-bound transitions are included in the summation. This has the consequence that subshell amplitudes show resonance structures wherever the photon energy equals a bound-bound transition energy. The resonances corresponding to transitions to unfilled shells are real and will appear in the physical total atom amplitude. However, the resonances due to transitions to filled or partially filled bound states will be completely or partially canceled, when the total atom amplitude is evaluated, due to compensating contributions in the scattering from those filled states.

As an illustration of these resonance features, we show in Fig. 6 the K-shell forward scattering amplitude for the cases of Ne^{6+} and Ne^{9+}. For Ne^{6+}, the first two resonances at $\omega/\omega_K=0.823$ and 0.925 correspond to $K\rightarrow L_{2,3}$ and $K\rightarrow M$ transitions. As the degree of ionization increases, the size of the resonance region increases and also the separation between resonances. This is due to the fact that increased ionization makes the atom more Coulombic and less screened; binding energies and binding-energy differences increase.

We have compared our result for the hydrogenic case (Ne^{9+}) with the NRDA result of Gavrila. The agreement is quite good. In other ions one sees departures from the Coulombic situation. However, for higher energies the K-shell amplitude for neutral atoms agrees with Gavrila's calculation,[6] particularly if one includes screening normalization corrections to the anomalous amplitudes.

In the present calculation the finite lifetime of the excited states was not taken into account, and so the resonances are infinitely sharp. For resonances involving filled shells this does not affect the total atom amplitude, in view of the cancellation mentioned earlier, as long as both canceling contributions are calculated with sufficient accuracy. We have examined the shape of the resonance region $K\rightarrow L_{2,3}$, for different degrees of ionization, by fitting the amplitude to its expected functional form

$$C_1+C_2/[\omega-(\omega_K-\omega_{L_{2,3}})]\ .$$

The parameter C_2 measures the oscillator strength of the transition under consideration. In the case of Ne, C_2 changes by a factor of 2.5 between neutral Ne and hydrogenic Ne^{9+}. This demonstrates that as the system becomes more Coulombic, the oscillator strength increases.

III. L-SHELL AMPLITUDES

The L-shell amplitudes should be smooth through the energies in the neighborhood of the K edge and above. However, since we calculate the amplitudes independently, we introduce into the L-amplitudes spurious resonances corresponding to transition to the K shell. Except for these resonance parts, the real L amplitude is within a few percent of the form-factor value for the energies under consideration here. We can approximate each L-subshell amplitude as

$$A_L=A_L^{\rm ff}+\sum\frac{\langle L\,|\,\mathbf{e}_f^*\cdot\boldsymbol{\alpha}e^{-i\mathbf{k}_f\cdot\mathbf{r}}\,|\,b\rangle\langle b\,|\,\mathbf{e}_i\cdot\boldsymbol{\alpha}e^{i\mathbf{k}_i\cdot\mathbf{r}}\,|\,L\rangle}{\omega-E_{Lb}}\ ,$$

where ω is the photon energy, the summation is over all the bound states b, E_{Lb} is the corresponding transition energy, and $A_L^{\rm ff}$ is the form-factor amplitude. The $\boldsymbol{\alpha}$ are the usual Dirac matrices.

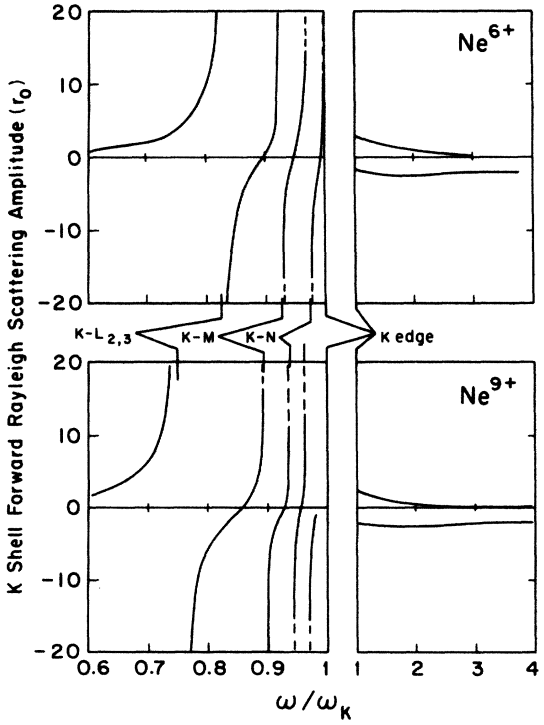

FIG. 6. K-shell forward Rayleigh scattering amplitudes for Ne^{6+} and Ne^{9+} showing some details in the resonance region.

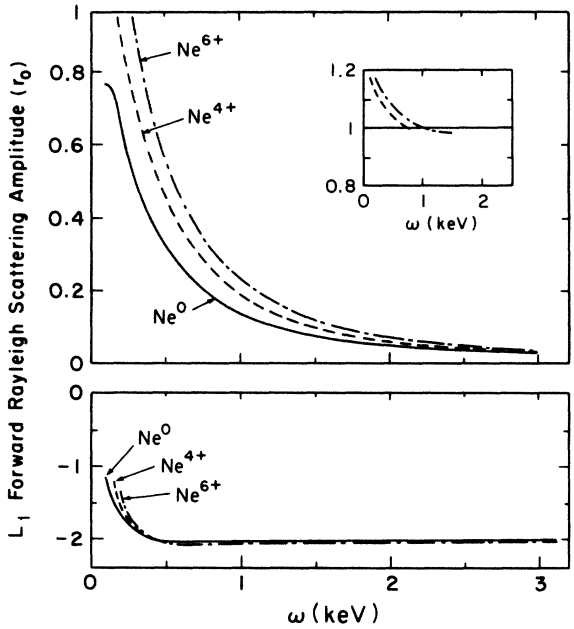

FIG. 7. Real and imaginary parts of L_1-subshell forward Rayleigh amplitudes for Ne^0, Ne^{4+}, and Ne^{6+}. The inset shows the ratio of L_1 imaginary amplitude for a given ion to that of the neutral case multiplied by the inverse ratio of the wave-function normalization constants squared plotted against ω.

The $L_1 \rightarrow 1s$ transition is forbidden in dipole approximation and other bound-bound transition energies involving L_1 are small (less than 100 eV). Hence, beyond the K edge, to a good approximation, the real part of the L_1 amplitude is a smoothly varying quantity whose value is very close to the form factor value $2r_0$ (Fig. 7), independent of degree of ionization. Note that the L_1 threshold moves from 40 eV for Ne^0 to 203 eV for Ne^{6+}. Hence breakdown of the common form-factor value may be expected at progressively higher energies for higher ionization.

Figure 7 also shows the corresponding situation for the L_1 imaginary amplitudes. Increasing ionization increases the amplitude at a given photon energy. In the regions sufficiently far from the respective thresholds, the ratio of different ionization amplitudes varies slowly and approaches the wave-function normalization ratio squared for energies more than about 5 times the L_1 threshold energy, as has been predicted by Pratt and Tseng.[7] This is shown in the inset of Fig. 9 for the case of neon. In this inset, the ratio of L_1 imaginary amplitude for a given ion to that of the neutral case multiplied by the inverse ratio of the wave-function normalization squared is plotted against ω. The small anomalous real amplitude would be expected to have a similar behavior.

In the case of the L_2 amplitude, the $L_2 \rightarrow K$ transition is allowed in dipole approximation and leads to a resonant term which exactly cancels the corresponding term in the K-shell amplitude. Figure 8 shows the situation for the Ne^0 and Ne^{4+} cases. As for L_1, resonances corresponding to $L_2 \rightarrow$ higher shell transitions occur at much lower energies and do not affect the region investigated here. While the observed resonance in the K-shell amplitude (as in Fig. 6) is due to both $K \rightarrow L_2$ and $K \rightarrow L_3$ transitions (which have not been separated) the resonance in Fig. 8 only corresponds to the $L_2 \rightarrow K$ transition. Consequently, in fitting the resonance with parameters C_1 and C_2, the value of C_2 is smaller by a factor of 3.

The L_3 subshell amplitude is relevant only in those cases for which L_3 is occupied, as in the Ne^0 and C^0 cases. (In the case of carbon we have employed the occupation numbers $\frac{2}{3}$ for L_2 and $\frac{4}{3}$ for L_3 as used by Scofield in his photoeffect cross-section evaluation.[8]) The general features of the L_3 amplitude are similar to those of the L_2 amplitude.

IV. TOTAL AMPLITUDES AND CROSS SECTIONS

In the independent particle approximation the total atom amplitude is simply the algebraic sum of the individual subshell amplitudes with due weighting of the occupation numbers. Total cross sections obtained for neon have been shown in Figs. 1 and 2. In Fig. 9 we show 0° and 180° total cross section for C^0, C^{2+}, and C^{4+}. First we consider forward cross sections for Ne^0 and C^0. As the L_2 and L_3 subshells are only partially filled in C^0, the K-shell $K \rightarrow L_{2,3}$ resonance component is only partially canceled by L_2, L_3 resonance components. But the L shell is filled in Ne and so the cancellation is complete. In the absence of resonances, the dominant real contribution below the K threshold is from the L-shell form-factor contribution, which is negative in sign. Near resonance, the uncanceled positive part of the K-shell $K \rightarrow L_{2,3}$ resonance amplitude interferes destructively with this background form factor contribution. The cross section plunges to a very low minimum value (Fano profile) below the $K \rightarrow L$ transition energy in the case of carbon. In the case of Ne, since the L_2 and L_3 subshells are filled, the cross section would show such a dip only much closer to the K threshold, just below the $K \rightarrow M$ resonance transition energy.

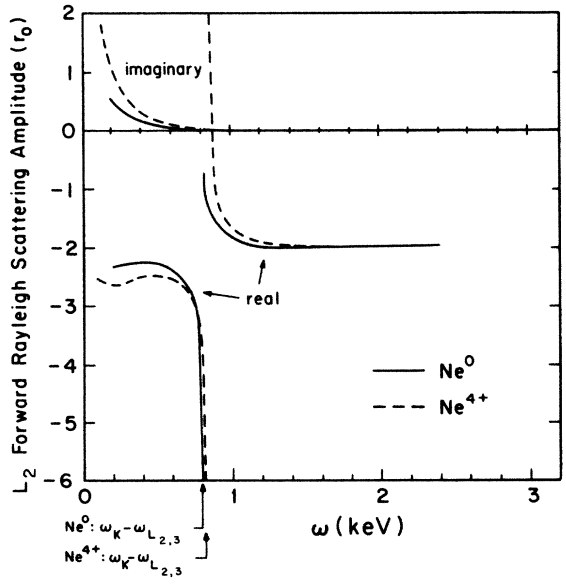

FIG. 8. Real and imaginary parts of forward Rayleigh scattering amplitudes from the L_2 subshell of Ne^0 and Ne^{4+}.

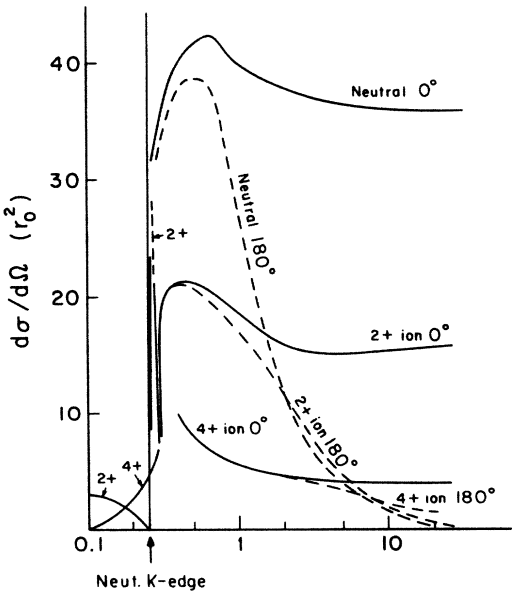

FIG. 9. Total atom cross sections for C^0, C^{2+}, and C^{4+} at 0° and 180°.

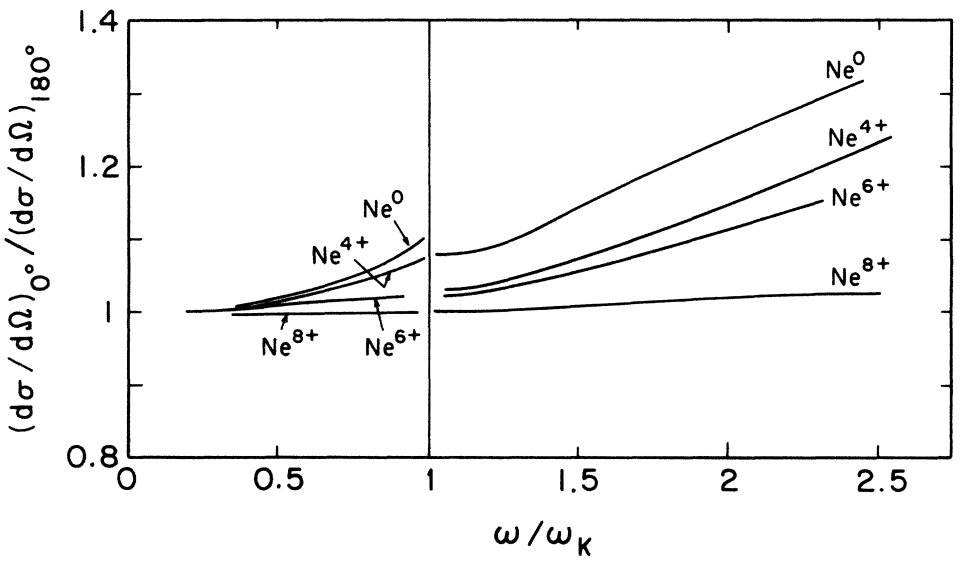

FIG. 10. Ratio of forward-to-backward cross sections for Ne^0, Ne^{4+}, Ne^{6+}, and Ne^{8+} as a function of ω/ω_K.

As the degree of ionization increases, more nearby bound states become available as intermediate states; the resonances and their preceeding minima appear in the total cross section. The energy grid of our calculations is not adequate to show the energy dependence in this resonance region in full detail. However, the appearance of the $K \rightarrow L_{2,3}$ resonance peak in the cross section for ions is clear enough to be seen. We refer again to Fig. 1, which compares (except in the resonance region) the resulting total forward scattering cross section for various degrees of ionization in neon. It is clear that, except near the K edge, the primary effect of ionization on the total cross section arises from the reduction in the number of electrons present from which scattering can occur. However, a far more complex set of changes occurs with ionization, near threshold.

V. ANGULAR DEPENDENCE OF AMPLITUDES AND TOTAL CROSS SECTIONS

In the preceding sections, the discussion of amplitudes and cross sections has primarily been for forward scattering. In the situations we have considered $A_{\parallel}$ is nearly equal to $A_{\perp}\cos\theta$, implying that B is small in Eq. (1). However, $A_{\perp}$ itself does have angular dependence, varying from slight to significant, depending on the subshell and the energy region. This reflects deviations from dipole approximation. In this section we discuss the angular dependence of the amplitude $A_{\perp}$ and the total cross section, and how that dependence changes with ionization.

For $\omega < \omega_K$, the K-shell amplitudes are essentially dipolar in character. For $\omega > \omega_K$, but close enough to ω_K, the imaginary part is again dipolar. We chose the ratio $A(\theta=180°)/A(\theta=0°)$ as a measure of departure from the dipole character. In this measure, up to about 5 keV ($\sim 6\omega_K$ for Ne^0 and $4\omega_K$ for Ne^{9+}) the departure is less than 1%. This can be understood from the fact that the characteristic K-shell electron momenta range from 5.7×10^{-2} mc (in Ne^0) to 7.3×10^{-2} mc (in Ne^{9+}) and the maximum momentum transfer implied in 180° scattering of a 5-keV photon is $\sim 2\times10^{-2}$ mc. For carbon and its ions the K-shell characteristic momenta are of course smaller and so the 1–2% level departures from dipole character occur at correspondingly lower values of ω (by nearly a factor of 3).

In the case of L-shell amplitudes, since we are looking farther above their thresholds, all the imaginary amplitudes are much smaller in magnitude in comparison with the real amplitudes. Their departure from dipole character, while somewhat larger at the upper limit of the energy regime under consideration, does not contribute to the angular dependence of the total amplitude. However, the real parts of the L-shell amplitudes do have angular dependence, small to significant depending on the subshell and the element. The main reason for this angular dependence of L-shell real amplitudes is that, for the higher energies, the momentum transfer in back scattering becomes comparable with the characteristic L-shell electron momenta. For example, at $\omega=2.5\omega_K$, the departure from the dipolar character in L_1 and L_2 amplitudes ranges from less than 10% for Ne^0 to about 15% for Ne^{6+}. In the case of the L_3 amplitude the corresponding departure is ~25%. The stronger angular dependence of the L_3 amplitude is due to the relatively low characteristic momenta in that subshell ($\sim 0.8\times10^{-2}$ mc in Ne and 0.6×10^{-2} mc in C). These departures from dipole character affect the angular distribution of the total cross section in the neutral atoms considered here.

The deviation of total atom cross sections from dipole character is presented in Fig. 10. This deviation becomes smaller with increasing ionization, reflecting the increasingly dipolar character of the innermost subshells at fixed energy.

*Permanent address: Department of Physics, Indian Institute of Technology, Powai, Bombay 400076, India.

†Permanent address: Test Planning and Diagnostics Division, Sandia National Laboratory, Albuquerque, New Mexico 87185.

‡Permanent address: Department of Physics, Bose Institute, Calcutta 700009, India.

§Permanent address: North Bengal University, Darjeeling 734430 India.

[1]L. Kissel, R. H. Pratt, and S. C. Roy, Phys. Rev. A **22**, 1970 (1980).

[2]John C. Parker, G. W. Reynaud, David J. Botto, and R. H. Pratt (unpublished).

[3]L. Kissel and R. H. Pratt, in *Atomic Inner-Shell Physics,* edited by B. Crasemann (Plenum, New York, 1985), pp. 465—532.

[4]P. P. Kane, Lynn Kissel, R. H. Pratt, and S. C. Roy, Phys. Rep. (to be published).

[5]M. Gavrila, Phys. Rev. **163**, 147 (1967).

[6]S. C. Roy and R. H. Pratt, Phys. Rev. A **26**, 651 (1982).

[7]R. H. Pratt and H. K. Tseng, Phys. Rev. A **5**, 1063 (1972).

[8]J. H. Scofield, University of California Radiation Laboratory Report No. 51326, 1973 (unpublished).